Graph Ricci Curvatures Reveal Disease-related Changes in Autism Spectrum Disorder

Pavithra Elumalai,[1,*] Yasharth Yadav,[1,2,*] Nitin Williams,[3,4,†] Emil Saucan,[5] Jürgen Jost,[6,7] and Areejit Samal[1,8,‡]

[1] *The Institute of Mathematical Sciences (IMSc), Chennai, India*
[2] *Indian Institute of Science Education and Research (IISER), Pune, India*
[3] *Helsinki Institute of Information Technology, Department of Computer Science, Aalto University, Finland*
[4] *Department of Neuroscience & Biomedical Engineering, Aalto University, Finland*
[5] *Department of Applied Mathematics, ORT Braude College, Karmiel, Israel*
[6] *Max Planck Institute for Mathematics in the Sciences, Leipzig, Germany*
[7] *The Santa Fe Institute, Santa Fe, NM, USA*
[8] *Homi Bhabha National Institute (HBNI), Mumbai, India*

Autism Spectrum Disorder (ASD) is a set of neurodevelopmental disorders that pose a significant global health burden. Measures from graph theory have been used to characterise ASD-related changes in resting-state fMRI functional connectivity networks (FCNs), but recently developed geometry-inspired measures have not been applied so far. In this study, we applied geometry-inspired graph Ricci curvatures to investigate ASD-related changes in resting-state fMRI FCNs. To do this, we applied Forman-Ricci and Ollivier-Ricci curvatures to compare networks of ASD and healthy controls (N = 1112) from the Autism Brain Imaging Data Exchange I (ABIDE-I) dataset. We performed these comparisons at the brain-wide level as well as at the level of individual brain regions, and further, determined the behavioral relevance of region-specific differences with Neurosynth meta-analysis decoding. We found brain-wide ASD-related differences for both Forman-Ricci and Ollivier-Ricci curvatures. For Forman-Ricci curvature, these differences were distributed across 83 of the 200 brain regions studied, and concentrated within the Default Mode, Somatomotor and Ventral Attention Network. Meta-analysis decoding identified the brain regions showing curvature differences as involved in social cognition, memory, language and movement. Notably, comparison with results from previous non-invasive stimulation (TMS/tDCS) experiments revealed that the set of brain regions showing curvature differences overlapped with the set of brain regions whose stimulation resulted in positive cognitive or behavioural outcomes in ASD patients. These results underscore the utility of geometry-inspired graph Ricci curvatures in characterising disease-related changes in ASD, and possibly, other neurodevelopmental disorders.

Keywords: resting-state fMRI; ASD; functional connectivity networks; Forman-Ricci curvature; TMS; tDCS

INTRODUCTION

Autism spectrum disorder (ASD) is an umbrella term for a diverse group of clinical presentations of neurodevelopmental disorders such as Autism, Asperger's syndrome, childhood disintegrative disorder and pervasive developmental disorder not otherwise specified (PDD-NOS) [1]. ASD is characterized by difficulties in social interaction, speech and non-verbal communication, restrictive/repetitive behaviors and varying levels of intellectual disability, and can also be accompanied by neurological or psychiatric disorders [1, 2]. Being highly heritable [2, 3], the prevalence of ASD is globally increasing, affecting 1 in 54 children aged 8 years in the United States [4] and 1 in 100 children aged under 6 years in India [5]. In 1990, ASD was declared as a disability in the United States. While an early diagnosis is key for early intervention, an accurate and effective diagnosis of ASD is crucial [6]. In order to provide a proper diagnosis and to better characterize the disorder, several studies have been undertaken to understand the pathophysiology and neurobiology of ASD (see e.g. Lord *et al.* [2] for a comprehensive review).

Neuroimaging methods like diffusion tensor imaging, magnetic resonance imaging (MRI) and functional magnetic resonance imaging (fMRI) are well recognised and enable us to understand structural and functional brain development in people with ASD compared to typical development, and to identify the disrupted neural mechanisms underlying ASD [7–10]. It also provides a means to validate clinical symptoms and cognitive theories of ASD neurobiologically [2, 7, 11]. fMRI captures activations in different regions of the brain through the changes in blood oxygen levels (BOLD signals) and the temporal correlations between these BOLD signals are referred to as functional connectivity in the brain [12]. Distant regions in the brain are activated synchronously even during rest [13, 14] and they form the resting state functional connectivity of the brain. Resting state functional MRI (rs-fMRI) studies that require participants to

* These authors contributed equally to this work
† Correspondence: nitin.williams@aalto.fi
‡ Correspondence: asamal@imsc.res.in

look at a blank screen with no task demands have been used to study resting state functional connectivity in the human brain, and have been demonstrated to be a convenient paradigm to identify neuronal correlates of neuropsychiatric disorders such as ASD [8, 11]. Alongside individual studies, data sharing initiatives like the Autism Brain Imaging Data Exchange (ABIDE) have offered large datasets of rs-fMRI images, encouraging and accelerating research on ASD [2, 11, 15].

Graph theory and network analysis provide objective, data-driven measures to analyse the topological architecture and connectivity patterns (human 'connectome') in the human brain [11, 16–20] and can provide us with deeper insights about the functional, structural and causal organization of the brain [20]. Remarkably, many previous studies on ASD have utilized graph-theoretic analysis of rs-fMRI functional connectivity networks (FCNs) to differentiate ASD from healthy [15, 21–29], and furthermore, some of these studies [15, 21, 27, 28] made use of the ABIDE I dataset. These studies investigated network characteristics such as small-worldness, modularity, clustering, efficiency, rich club organization and connection densities of the FCNs in ASD versus typical development, and reported abnormal functional organization in ASD both globally and at the level of nodes.

In recent years there has been an increasing interest in the development of geometric tools for analyzing complex networks [30], which enables the study of higher-order correlations in networks beyond pairwise interactions [31–33]. A fundamental concept in geometry is Ricci curvature [34], which quantifies the extent to which a space differs from being flat. Various nonequivalent definitions of graph Ricci curvature have been proposed [35–39] with an aim to capture the key properties of the classical Ricci curvature. Different notions of graph Ricci curvature have found applications in diverse areas, such as differentiating gene co-expression networks of cancer cells and healthy cells [40], identifying crashes and bubbles in financial networks [41, 42], and community detection in complex networks [43, 44]. Ollivier-Ricci curvature (ORC) [37] and Forman-Ricci curvature (FRC) [36, 38] are two widely used notions of graph Ricci curvature.

Notably, graph Ricci curvatures have also been applied to structural and functional connectivity networks of the human brain. Farooq *et al.* [45] applied ORC to brain structural connectivity networks to identify robust and fragile brain regions in healthy subjects. They also show that ORC can be used to identify changes in brain structural connectivity related to ASD and healthy aging. Simhal *et al.* [46] used ORC to measure changes in brain structural connectivity of individuals with ASD before and after the infusion of autologous umbilical cord blood. ORC has also been used to study differences in brain structural connectivity networks of cognitively impaired and non-impaired multiple sclerosis patients [47]. Recently, Chatterjee *et al.* [48] used a version of FRC to determine the changes in brain functional connectivity related to attention deficit hyperactivity disorder (ADHD). Additionally, FRC has been used to analyze task-based fMRI data [49] as well as to predict intelligence of healthy human subjects [50]. Most of these studies have also contrasted graph Ricci curvatures with standard network measures such as clustering coefficient and node betweenness centrality, and showed that graph Ricci curvatures can provide new information about brain connectivity organization. However, a systematic evaluation of the association between graph Ricci curvatures of brain functional connectivity networks and the behavioral and cognitive symptoms of neurodevelopmental disorders such as ASD is lacking.

In the present work, we expand the scope of curvature-based analysis for characterizing brain connectivity by systematically applying graph Ricci curvatures to analyse abnormal functional connectivity network organization in ASD. Notably, we have utilized fMRI images of 1112 subjects from the ABIDE-I dataset and implemented a uniform preprocessing pipeline for each image in order to improve the reliability of our results. We employ FRC and ORC to compare the FCNs of individuals with ASD relative to age-matched healthy controls, and evaluate the role of these curvature measures as indicators of abnormal functional connectivity in ASD. For this purpose, we first analyze the brain-wide changes in functional connectivity by comparing average edge curvatures across the two groups. Second, we analyze the region-specific changes in functional connectivity by comparing node curvatures across the two groups. Third, we interpret the results of node-level comparisons for each resting state network (RSN) separately, in terms of the behavioral significance of brain regions showing differences in node curvature. Finally, we demonstrate a correspondence between the set of brain regions with altered curvature in ASD patients and the set of brain regions whose non-invasive stimulation with transcranial magnetic stimulation (TMS) [51] and transcranial direct current stimulation (tDCS) [52] have been reported in the literature to have a positive effect on ASD symptoms.

METHODS

In this section, we describe the methodology used to construct, analyze and compare the resting state functional connectivity networks (FCNs) of individuals with autism spectrum disorder (ASD) and healthy controls (HC), from raw resting-state functional MRI (rs-fMRI) images acquired from the Autism Brain Imaging Data Exchange I (ABIDE-I) project [15]. First, raw rs-fMRI data were spatially and temporally preprocessed using the CONN functional connectivity toolbox [53]. Second, we parcellated the brain into 200 distinct regions of interest (ROIs) or nodes

using the Schaefer atlas [54] and a 200×200 functional connectivity (FC) matrix was generated for each subject. Third, we filtered the FC matrix using a maximum spanning tree (MST) based approach followed by sparsity-based thresholding to construct FCNs for each subject. Fourth, we performed global- and local-level network analysis to compare the FCNs in the ASD group and the HC group. Fifth, we interpreted the behavioral relevance of the results from local analysis using Neurosynth-based meta-analysis [55, 56] and studied the relationship between node-level network measures and clinical scores.

Participants and imaging dataset

From the ABIDE-I project [15], we obtained raw rs-fMRI and anatomical data for 1112 participants (age range $= 7 - 64$ years, median $= 14.7$ years), out of which 539 individuals had autism spectrum disorder (ASD) and 573 were age-matched healthy controls (HC). ABIDE-I project is an international effort by 17 imaging sites that have collectively shared rs-fMRI, anatomical and phenotypic data. Further details such as MRI modalities and scan parameters are available on the ABIDE website: `http://fcon_1000.projects.nitrc.org/indi/abide`.

Quality assessment and exclusion criteria before preprocessing

We used the following criteria to exclude subjects in ABIDE-I from this study. First, the subjects with missing anatomical or functional files were excluded. Second, all subjects from the imaging site Stanford were excluded as it is the only site with spiral image acquisition protocol. Third, all subjects from the imaging site Leuven-1 were excluded due to unknown repetition times for the functional scans. Fourth, to assess the quality of the raw images in ABIDE-I, we have used the information on raters' decision available from the Preprocessed Connectome Project (PCP) [58], and the subjects whose raw image quality was described as 'fail' by both the raters were excluded. Note that we did not exclude the subjects based on IQ or match the cohorts for IQ in order to ensure that the results of our analyses are generalizable to the typical ASD population [15, 59]. After removing subjects based on the quality assessment (QA) checks and exclusion criteria described above, we were left with 494 subjects in the ASD group and 520 subjects in the HC group (Supplementary Table S1).

Raw fMRI data preprocessing

We used the CONN functional connectivity toolbox [53] to process the rs-fMRI data from ABIDE-I. Figure 1 is a schematic summarizing the processing pipeline for rs-fMRI data used in this study. We have created a protocol video providing a visual guide to rs-fMRI preprocessing using CONN toolbox which is available at: `https://www.youtube.com/watch?v=MJG8-oUsLqg`

Spatial preprocessing

We performed motion correction, slice-timing correction, outlier detection, and structural and functional segmentation and normalization. First, the functional images were co-registered to the first scan of the first session. The SPM12 realign and unwarp procedure [60] was used to realign and motion correct the images using six rigid body transformation parameters: three translations in x, y and z directions, and three rotations namely pitch, yaw and roll. Second, the SPM12 slice-timing correction procedure [61] was used to temporally align the functional images. Third, Artifact Detection Tools (ART)-based outlier detection was performed where acquisitions with framewise displacement greater than 0.5 mm or global BOLD signal changes greater than 3 standard deviations were marked as outliers. Fourth, segmentation and normalization [62] was carried out to normalize the images into the standard Montreal Neurological Institute (MNI) space, and then, segment the brain into grey matter, white matter and cerebrospinal fluid (CSF) areas. Raw T1-weighted volume of the anatomical image and mean BOLD signal of the functional images were used as reference in this step. Subjects with bad image quality and signal dropouts in their scans or subjects with registration or normalization errors were excluded from further analysis.

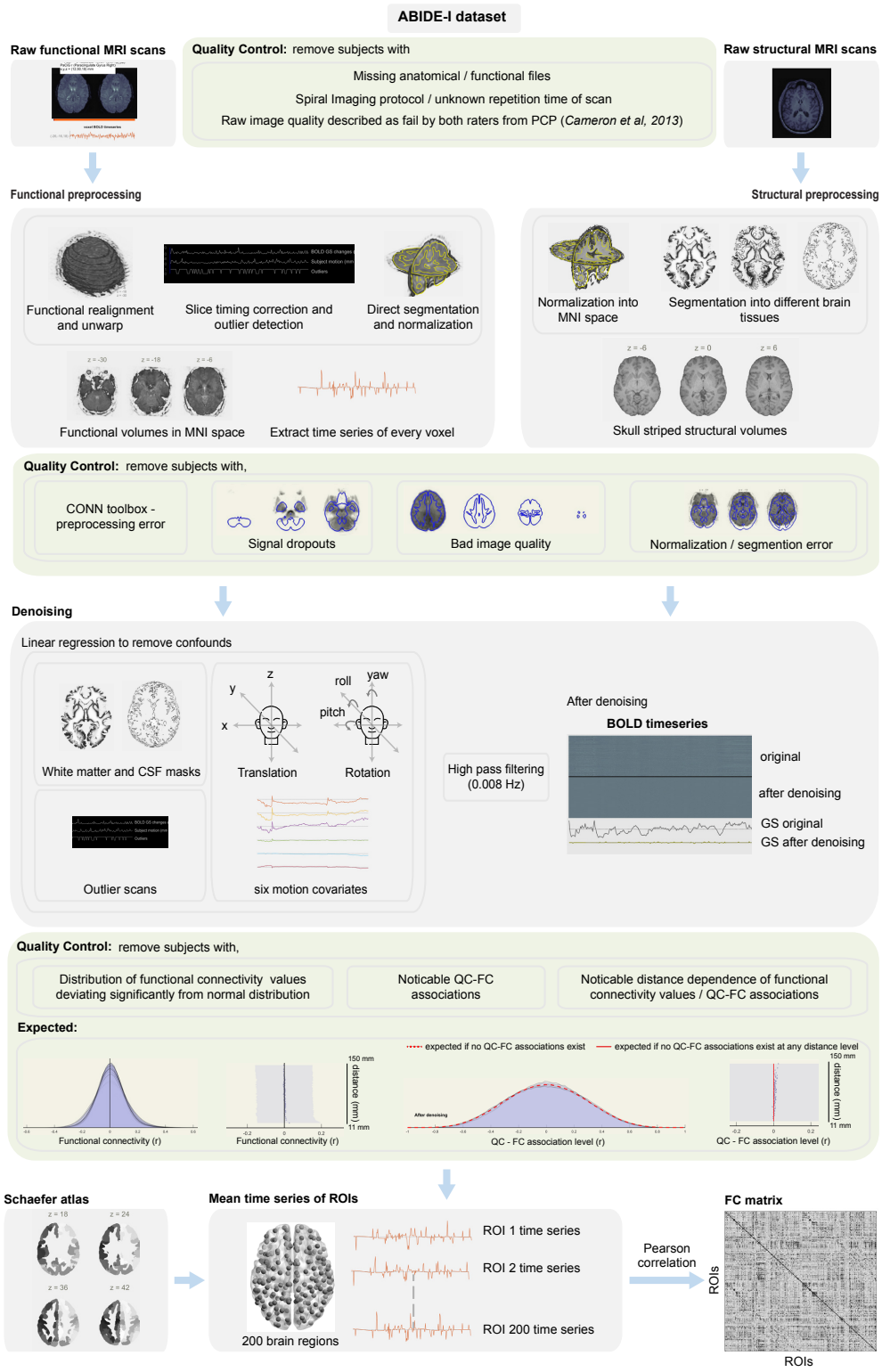

FIG. 1. A schematic diagram summarizing the rs-fMRI processing pipeline employed in this study. The raw fMRI scans undergo four steps in spatial preprocessing, namely, motion correction, slice-timing correction, outlier detection, and direct segmentation and normalization. The raw structural MRI scans are normalized to the Montreal Neurological Institute (MNI) space, and segmented into grey matter, white matter and cerebrospinal fluid (CSF) areas. In the temporal preprocessing or denoising step, the BOLD time series of each voxel is extracted and the remaining physiological and motion confounds are removed using linear regression. The confounds include white matter and CSF masks, subject-motion parameters and outlier scans. The residual BOLD time series of each voxel undergoes a high-pass filtering at 0.008 Hz. The Schaefer atlas is used to parcellate the brain into 200 regions of interest (ROIs) and the mean time series for each ROI is computed. Finally, Pearson correlation coefficient is computed between all pairs of ROIs, resulting in a 200 $\times$ 200 functional connectivity (FC) matrix. Thorough quality assessment (QA) checks were implemented both before and after preprocessing. In this figure, the head icon under denoising section is made by Freepik from flaticon.com [57].

Characteristics	ASD Group	HC Group
number of subjects	395 (44 female)	425 (78 female)
age (in years)		
mean ± s.d.	15.6 ± 7.1	15.51 ± 6.23
range	$7 - 58$	$6 - 57$
handedness (n)		
left	29	27
right	225	247
mixed	3	3
ambidextrous	1	0
ADI-R Social		
mean ± s.d.	19.72 ± 5.25	–
range	$7 - 30$	–
ADI-R Verbal		
mean ± s.d.	15.95 ± 4.25	–
range	$2 - 26$	–

TABLE I. Summary of demographic and clinical information for the 820 subjects from ABIDE-I project that fulfil the inclusion criteria and were selected for network analysis in this study. 395 subjects belong to the autism spectrum disorder (ASD) group and 425 subjects belong to the healthy control (HC) group. The subjects in both the groups are age-matched ($p = 0.835$). Handedness data were missing for 137 ASD and 148 HC subjects. ADI-R social data were missing for 120 ASD participants. ADI-R verbal data were missing for 119 ASD participants.

Denoising

After the spatial preprocessing of the raw rs-fMRI scans, the BOLD time-series associated with each voxel was extracted using the CONN toolbox. Next, we performed temporal preprocessing or denoising using the CONN toolbox to further reduce physiological or motion effects from the BOLD time-series. First, we implemented anatomical component-based noise correction procedure (aCompCor), to simultaneously remove five potential noise components [63] each from white matter and CSF areas, 12 potential noise components from estimated subject motion parameters and their associated first-order derivatives [64], and one noise component from each of the identified outlier scans (scrubbing) [65] in a single linear regression step. Second, a high-pass filtering was performed to remove temporal frequencies below 0.008 Hz from the BOLD time-series.

Quality assessment and exclusion criteria after preprocessing

After preprocessing the raw fMRI data, we applied the following criteria to exclude participants from the analysis. Subjects were excluded if the FC distribution deviated significantly from normal distribution, or if the FC distribution showed a noticeable distance dependence [66]. We additionally excluded subjects that showed a noticeable correlation between quality control (QC) variables and FC values, or if the QC-FC correlations showed a noticeable distance dependence [66]. After removing subjects based on these exclusion criteria, we were left with 395 subjects in the ASD group and 425 subjects in the HC group (Supplementary Table S1). The FC matrices of these remaining 820 subjects were used for network analysis. The demographic and clinical information for these subjects from ABIDE-I included in our study are summarized in Table I.

Atlas-based definition of nodes and functional connectivity matrix construction

A widely used approach for defining nodes in functional connectivity networks (FCNs) is to group closely related neighboring voxels into cortical parcels, in order to obtain nodes with interpretable neurobiological meaning [67]. Furthermore, the use of brain parcellations also reduces the computational load of further analyses. In this study, we used a predefined cortical parcellation atlas by Schaefer *et al.* [54], which is based on a gradient-weighted Markov random field approach. While the Schaefer atlas is available at multiple resolutions, we considered the resolution that parcellates the brain into 200 distinct regions of interests (ROIs) wherein each hemisphere comprises 100 ROIs. In this parcellation, each ROI belongs to one of seven resting state networks (RSNs), namely, 'visual', 'somatomotor', 'dorsal attention', 'salient ventral attention', 'limbic', 'control', and 'default'. Using the CONN toolbox, the time series of each ROI was computed as the average of the time series of all the voxels that it contains. Subsequently,

Pearson correlation coefficient between the time series of every pair of ROIs was calculated in the CONN toolbox, which resulted in a 200×200 FC matrix for each subject.

Construction of sparsity-based functional connectivity networks

In the preceding subsection, we described the FC matrix which is a correlation matrix that can be represented as a complete, weighted and undirected graph wherein the ROIs correspond to the nodes and the weights of edges are given by the correlation values between ROIs. The construction of the FCN from the FC matrix of a subject includes two steps, namely maximum spanning tree (MST) construction and sparsity-based thresholding.

First, to extract the most important edges from the FC matrix, we constructed its MST using Kruskal's algorithm [68]. The MST is a spanning tree of the weighted graph with maximum edge weight. Note that the MST for a weighted graph with n nodes is an acyclic graph (more precisely, a tree) with $(n-1)$ edges which is always connected. Second, we used sparsity-based thresholding, wherein edges are iteratively added to the MST in decreasing order of their correlation values, until a resulting network with the desired sparsity was obtained. Further, the resulting network with desired sparsity was binarized by ignoring the edge weights before proceeding to compute the network properties [23, 69].

Evidently, this choice of MST construction followed by sparsity-based thresholding to generate the FCNs ensures that the constructed networks for different subjects are connected and have the same number of edges. Such networks enable direct mathematical comparison of global and local network properties across subjects [23, 70, 71]. We remark that this choice of MST followed by sparsity-based thresholding to construct FCNs from rs-fMRI images has been used earlier by Achard *et al.* [72].

As there is no rationale for using a specific graph density, previous studies [23, 26, 28] have explored network properties across a range of graph densities. In this work, we have studied the network properties over a wide range of graph densities between 0.02 or 2% edges and 0.5 or 50% edges, with an increment of 0.01 or 1% edges. Thus, for each of the 820 subjects from ABIDE-I considered in this study, we have constructed 49 unweighted and undirected networks. In other words, we have generated 820×49 FCNs for 820 subjects across 49 graph densities or thresholds for this study, and the constructed networks are available for download from: `https://github.com/asamallab/Curvature-FCN-ASD`.

Network-based analysis and statistical tests

As mentioned in preceding subsection, we constructed 49 unweighted and undirected networks with varying sparsity from the FC matrix corresponding to each subject, and thereafter, each of the 49 networks for a subject was characterized by computing discrete Ricci curvatures and other network properties. Specifically, we have focused here on two discrete Ricci curvatures, namely Forman-Ricci curvature (FRC) [36, 38, 39] and Ollivier-Ricci curvature (ORC) [37]. Notably, the two discrete Ricci curvatures are naturally defined for edges in a network and capture different aspects of the classical Ricci curvature [39]. Moreover, we have also explored here several standard global network measures including average clustering coefficient, modularity [73], average shortest path length, average node betweenness centrality, global efficiency [74] and average local efficiency [74]. In Supplementary Information, we describe the different global and local network measures employed here to characterize the FCNs.

To compare the global properties of the FCNs across the two groups (ASD versus HC), we first computed the average FRC of edges, average ORC of edges and seven other global network measures (including average clustering coefficient, modularity, average shortest path length, average node betweenness centrality, global efficiency and average local efficiency), for each of the 820×49 networks corresponding to the FC matrices of 820 subjects across 49 graph densities. To compare the node-level properties of the FCNs across the two groups (ASD versus HC), we computed the node FRC and node ORC for each of the 200 nodes in each of the 820×49 networks corresponding to the FC matrices of 820 subjects across 49 graph densities. Note that the node Ricci curvature is defined as the sum of edge Ricci curvatures for the edges incident on that node [39] (see Supplementary Information). Additionally, we computed two standard network measures, namely node clustering coefficient and node betweenness centrality.

For the global measures, we evaluated the differences between the two groups across the 49 graph densities in the range $2-50\%$ considered in this study by using a two-tailed two-sample t-test, and moreover, we used a false discovery rate (FDR) correction [75] to correct for multiple comparisons and control the occurrence of false positives. Note that the α for this FDR correction was set to 0.05. For the node-level measures, we first computed the area under the curve (AUC) for a given node measure across the 49 graph densities considered in this study [26, 69]. Thereafter, we used a two-tailed two-sample t-test to evaluate the differences between the two groups via AUCs of the node measures for each of the 200 nodes in the network, and moreover, we used FDR correction to correct for multiple comparisons. Note that the α for this FDR correction was set to 0.05.

The computer codes for FRC and ORC are available at: `https://github.com/asamallab/Curvature-FCN-ASD`. The other global network measures mentioned above for FCNs were computed using the Python package NetworkX [76]. Furthermore, the statistical tests were performed in Python packages SciPy [77] and statsmodels [78].

Neurosynth meta-analysis and relationship with clinical scores

We used Neurosynth meta-analysis decoding to interpret the results of the node-based network comparisons, in terms of their behavioural relevance [56]. Corresponding to each node network measure studied here, we identified a set of nodes (ROIs) that showed significant differences between the ASD and HC groups. For a set of nodes with significant between-group differences for a network measure, we used Neurosynth meta-analysis tool [55] to find terms related to cognition, perception and behavior corresponding to the centroid coordinates of each ROI in the set. Further, we partitioned the set of identified ROIs which show significant between-group differences, by the 7 RSNs in the Schaefer atlas, and thereafter, the frequency counts of the terms associated with the subset of identified ROIs in a particular RSN were calculated. To determine statistical significance of these frequency counts, we calculated the frequency counts of the same terms associated with an equal size set of randomly selected surrogate ROIs, and thereafter, the z-score for the frequency counts of each term associated with the subset of original ROIs was calculated. Subsequently, the z-scores were converted into p-values assuming a normal distribution and an FDR correction with α equal to 0.05. This was done for each RSN separately, to identify those terms selectively associated with each of the 7 RSNs.

After identifying the set of nodes (or ROIs) that showed significant between-group differences in FRC (or ORC), we performed a post-hoc correlation analysis to find the relationship between FRC (or ORC) of the identified nodes and clinical scores related to symptom severity in the ASD group. Specifically, we chose two clinical scores based on the Autism Diagnostic Interview-Revised (ADI-R) scoring [79], which are: (i) ADI-R verbal and (ii) ADI-R social. We measured the relationship between the node FRC (or the node ORC) and the ADI-R scores by computing the partial correlations, with age and gender as covariates. Subsequently, we used an FDR correction with α equal to 0.05 to control the occurrence of false positives.

Identifying brain regions whose stimulation with non-invasive brain stimulation methods of ASD patients resulted in positive behavioral and cognitive outcomes

We performed a literature search to identify scientific papers reporting the effect of non-invasive brain stimulation (NIBS) on core symptoms of ASD, and then used results reported in these papers to identify those brain regions whose stimulation resulted in positive behavioral and cognitive outcomes. Figure 2 summarizes the workflow we employed to collect and classify the eligible articles. We used PubMed to perform the literature search. The search query to PubMed reflected diagnosis of interest including 'autism spectrum disorder', 'Asperger's syndrome', 'autism' and three major brain stimulation methodologies including 'Transcranial magnetic stimulation', 'TMS', 'transcranial direct current stimulation', 'tDCS', 'transcranial alternating current stimulation', 'tACS'. The search was performed in October 2021 and the exact details regarding the search query are provided in Table II. The PubMed search returned 235 articles.

We followed a three-stage procedure to further refine the list of 235 articles returned by the PubMed search. First, we checked for papers missing from the corpus generated by the PubMed search, by scanning review articles on the use of NIBS methods to study ASD. We also searched these review articles for potential databases of NIBS experiments on ASD. Second, we filtered the articles based on title and abstract, based on relevance. We defined relevance according to the following criteria. The inclusion criteria were: (1) studies on populations diagnosed with ASD, and (2) studies that have used non-invasive brain stimulation techniques namely, TMS (and its variants such as rTMS), tDCS and tACS, and (3) studies that have investigated the effect of NIBS on the core behavioral and cognitive symptoms of ASD, and (4) studies that are peer-reviewed. The exclusion criteria were: (1) review articles, (2) articles presented in languages other than English, (3) studies that did not perform NIBS, (4) studies that investigate new protocols for NIBS, (5) studies that report no positive effects in ASD symptoms post NIBS, (6) studies whose target areas for NIBS were not clearly reported, and (7) articles without access to full-text. Third, we classified the articles based on their stimulation technique (TMS/ tDCS/ tACS) and checked the full text of the articles for relevance, according to the same criteria as above. This process yielded 19 eligible articles for TMS, 12 eligible articles for tDCS and zero articles for tACS.

We identified Barahona-Corraa *et al.* [81] as a database of TMS studies in ASD published before 2018, with data collection guided by preferred reporting items for systematic reviews and meta-analysis (PRISMA) [80]. Similarly, we identified Garcia-Gonzalez *et al.* [82] as a database of tDCS studies in ASD published before August 2019, also

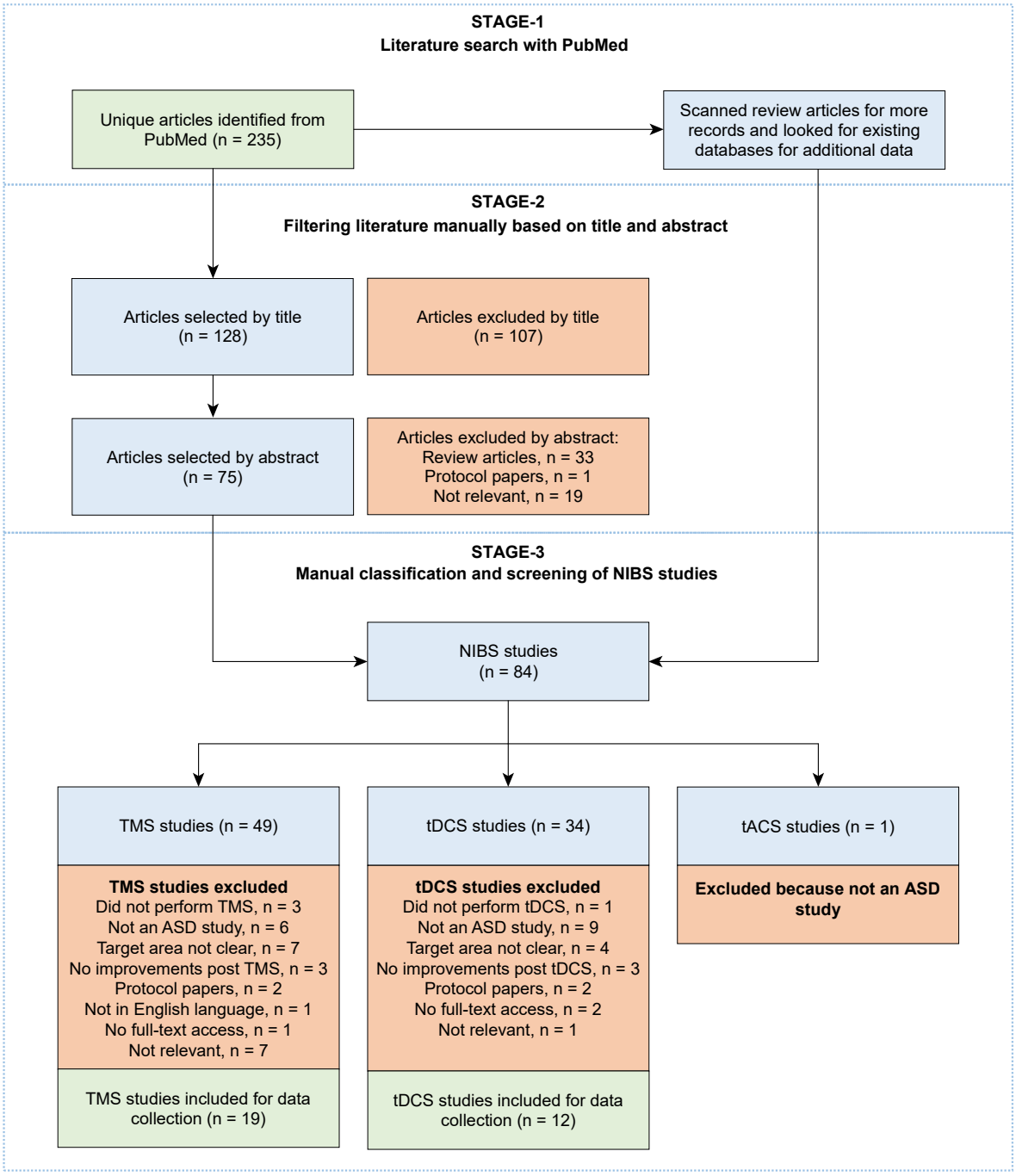

FIG. 2. Summary of the workflow employed to compile data from non-invasive brain stimulation (NIBS) experiments. The workflow is presented according to PRISMA statement [80]. First, we identified 235 potential records from PubMed. Second, we filtered the articles based on title and abstract. Third, we scanned review articles for more records and looked for existing databases for additional data. After performing the above steps, we were left with 84 potential NIBS studies. Finally, we classified the studies based on the stimulation technique (TMS/tDCS/tACS) and screened the studies individually for eligibility. We were left with 19 TMS studies and 12 tDCS studies, which were used to extract experimental data.

Search date	Search query	Search filters	Source
October 18, 2021	((transcranial magnetic stimulation) AND (autism)) OR ((transcranial magnetic stimulation) AND (Asperger)) OR ((transcranial magnetic stimulation) AND (PDD NOS)) OR ((transcranial direct current stimulation) AND (autism)) OR ((transcranial direct current stimulation) AND (Asperger)) OR ((transcranial direct current stimulation) AND (PDD NOS)) OR ((transcranial alternating current stimulation) AND (autism)) OR ((transcranial alternating current stimulation) AND (Asperger)) OR ((transcranial alternating current stimulation) AND (PDD NOS)) OR ((TMS) AND (autism)) OR ((TMS) AND (Asperger)) OR ((TDCS) AND (autism)) OR ((TDCS) AND (Asperger)) OR ((TACS) AND (autism)) OR ((TACS) AND (Asperger))	year : no filter, article attribute : no filter, language : no filter, age : no filter, sex : no filter, publication date: no filter	PubMed ($n = 235$)

TABLE II. Detailed summary of the electronic search query on PubMed that we used to obtain our original corpus of articles that perform non-invasive brain stimulation on ASD patients.

guided by PRISMA data collection. We utilized the data presented in these two databases along with the data that we extracted from the eligible articles in our corpus, such as author, publication year, DOI, number of participants, gender distribution, mean age, intellectual abilities, stimulation methodology and parameters, target areas, stimulation schedule, behavioral and cognitive outcome measures, behavioral and cognitive results, and any adverse reactions for the experiment group and the control group (if applicable). All the data collected are provided as Supplementary Tables S5 and S6. From these data, we identified the set of brain regions whose stimulation using these NIBS methods on ASD patients resulted in positive cognitive and behavioral outcomes.

Determining overlap between sets of regions identified from literature search of NIBS studies and those identified with graph Ricci curvatures

We determined the overlap between the sets of regions identified from literature search of NIBS studies and the sets of regions revealing ASD-related differences in graph Ricci curvatures of fMRI FCNs. The target areas described in the NIBS studies were cortical regions in the brain that are specified by their respective Brodmann areas [83] while we identified graph Ricci curvature differences in areas of the Schaefer 200 atlas. We used the MRIcron tool [84] to map each of the Brodmann areas to Schaefer ROIs, by identifying the Brodmann area encompassing the MNI centroid coordinates of each Schaefer ROI [85]. The mapping from Schaefer ROIs to the Brodmann areas is presented in Supplementary Table S7. Next, we compiled the set of Brodmann areas that serve as target areas from the eligible NIBS experiments and have shown a positive outcome, either behavioral or cognitive, as a result of stimulating that region. We then identified the set of Schaefer ROIs that were mapped to these Brodmann areas. From this set of Schaefer ROIs, we found the subset that yielded significant ASD-related differences according to the local graph Ricci curvatures namely, FRC and ORC, as well as for clustering coefficient and node betweenness centrality.

RESULTS

The primary goal of this study is to evaluate the utility of two notions of graph Ricci curvature, namely Forman-Ricci curvature (FRC) and Olivier-Ricci curvature (ORC), that have been recently ported to the domain of complex networks, as indicators of abnormal topological organization in resting state functional connectivity networks (FCNs) of individuals with autism spectrum disorder (ASD). For this purpose, we analysed spatially and temporally preprocessed rs-fMRI images of 395 individuals with ASD and 425 healthy controls (HC) as described in Methods section. Subsequently, 200 regions of interest (ROIs) or nodes were defined in the brain using the Schaefer atlas, and a 200×200 functional connectivity (FC) matrix was generated for each subject by computing the Pearson correlation coefficient between the time-series of all pairs of nodes. Thereafter, by combining maximum spanning tree (MST) and sparsity-based thresholding, we constructed FCNs over a wide range of graph densities between 0.02 or 2% edges and 0.5 or 50% edges, with an increment of 0.01 or 1% edges (see Methods). In a nutshell, we generated and analyzed 49 FCNs for each of the 820 subjects in the ABIDE-I dataset considered in this study.

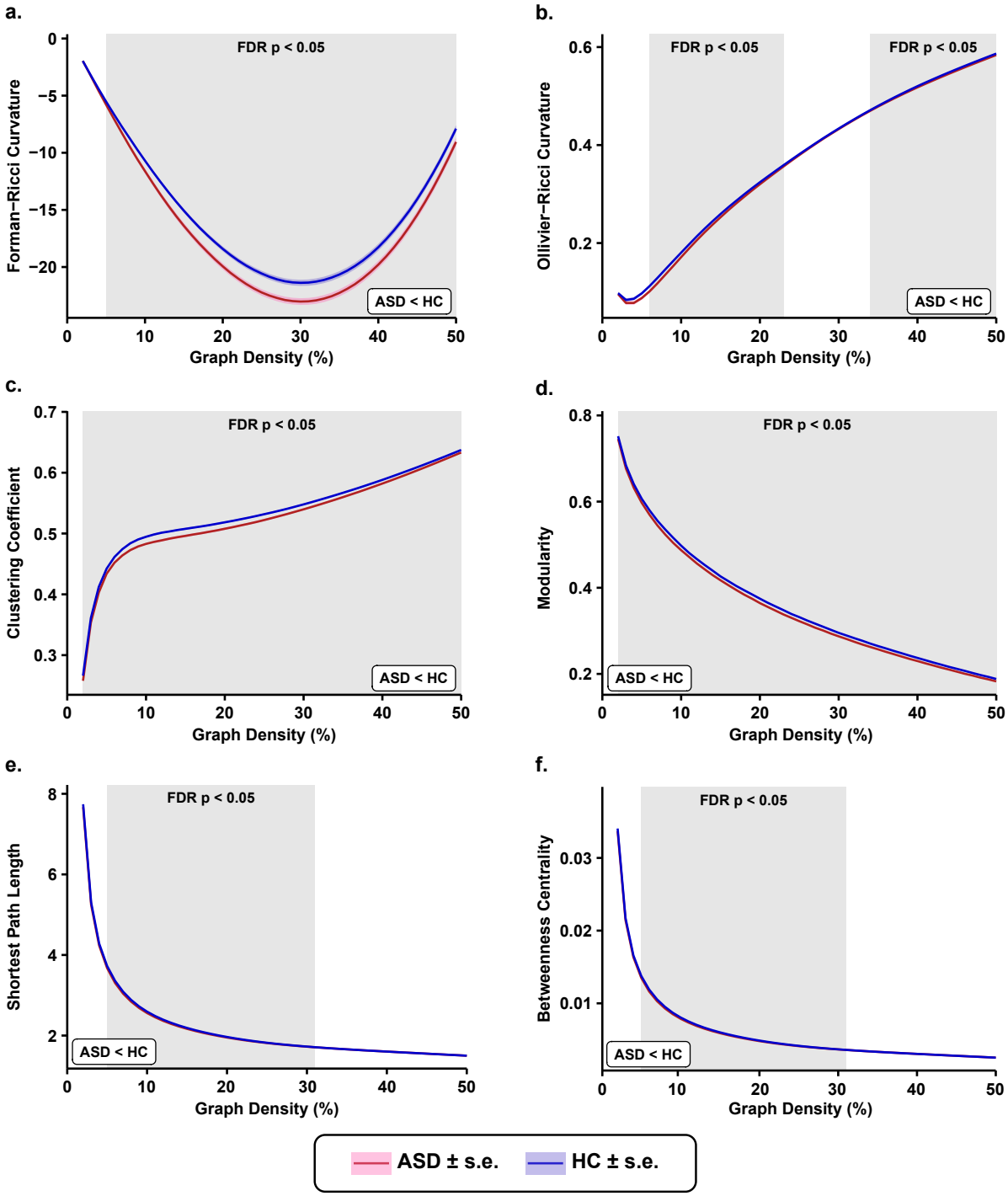

FIG. 3. Comparison plots of global changes in functional connectivity networks (FCNs) as captured by network measures between 395 subjects with autism spectrum disorder (ASD) and 425 age-matched healthy controls (HC). Each network measure was compared over a wide range of graph densities between 0.02 (i.e., 2% edges) and 0.5 (i.e., 50% edges), with an increment of 0.01 (i.e., 1% edges). The shaded regions in each plot indicate statistically significant differences ($p < 0.05$, FDR-corrected) between the two groups at the corresponding graph densities on the x-axis. Even though the differences are not explicit from the plots (e) and (f), the directionalities are programmatically verified. (a) Average Forman-Ricci curvature (FRC) of edges is significantly reduced in the ASD group across graph densities 5% - 50%. It is evidently the most visually observable difference among all the other network measures studied. (b) Average Ollivier-Ricci curvature (ORC) of edges is significantly reduced in the ASD group across graph densities 6% - 23% and 34% - 50%. (c) Average clustering coefficient is significantly reduced in the ASD group across all graph densities (2% - 50%). (d) Modularity is significantly reduced in the ASD group across all graph densities (2% - 50%). (e) Average shortest path length is significantly reduced in the ASD group across graph densities 5% - 31%. (f) Average node betweenness centrality is significantly reduced in the ASD group across graph densities 5% - 31%.

Brain-wide changes in functional connectivity networks

To investigate the differences in the global organization of FCNs between the ASD and HC groups, we computed the average edge FRC and average edge ORC across the 49 FCNs across the graph densities 2% - 50% for each subject. To compare the average edge curvatures at each graph density between the ASD and HC groups, we employed a two-tailed two-sample t-test followed by FDR correction (see Methods). In Figure 3a and Figure 3b, we show the differences in average edge FRC and average edge ORC, respectively, between the ASD and HC groups across the graph densities 2% - 50%. We find that average edge FRC is significantly lower ($p < 0.05$, FDR-corrected) in the ASD group compared to the HC group in the graph density range 5%-50% (Figure 3a). Similarly, we find that average edge ORC is lower ($p < 0.05$, FDR-corrected) in the ASD group compared to the HC group albeit the differences were insignificant ($p > 0.05$, FDR-corrected) in the graph density ranges 2%-5% and 24%-33% (Figure 3b). Although, the directionality of the differences with the two discrete Ricci curvatures is the same for the two groups, that is, average edge curvature in the ASD group is lower than that in the HC group, it is important to emphasize that the two discrete Ricci curvatures capture different aspects of the classical Ricci curvature, and thus, cannot serve as alternative measures across different types of networks. Specifically, ORC captures the volume growth property of the classical Ricci curvature whereas FRC captures the geodesic dispersal property [39]. While ORC has a deeper correspondence with the classical Ricci curvature, FRC is based on a simple combinatorial expression which is significantly faster to compute in larger networks. After comparing the average edge curvatures between FCNs of ASD and HC groups, we find that the statistical test (t-test followed by FDR correction) yielded lower p-values after FDR correction for average edge FRC compared to average edge ORC across most of the considered graph densities (Supplementary Table S2). In other words, the differences between FCNs for the two groups are more pronounced for the average edge FRC than average edge ORC.

To gain a deeper understanding of the altered global organization of FCNs between the ASD and HC groups, we also compared six other global network measures, namely, average clustering coefficient, modularity, average shortest path length, average node betweenness centrality, global efficiency and average local efficiency. We find that the average clustering coefficient is significantly lower ($p < 0.05$, FDR-corrected) in the ASD group compared to the HC group in the graph density range 2%-50% (Figure 3c). Moreover, our results for clustering coefficient are consistent with results from previous studies that have employed graph-theoretic measures to analyze resting state FCNs in ASD [23, 26, 28]. Thereafter, we find that the modularity of the FCNs is significantly reduced in the ASD group compared to the HC group in the graph density range 2%-50% (Figure 3d), and our results are consistent with the results from previous studies [23, 28]. Further, we find that the average shortest path length of the FCNs is significantly lower in the ASD group compared to the HC group in the graph density range 5%-31% (Figure 3e), and our results are consistent with results from previous studies [23, 26]. Lastly, we find that average node betweenness centrality is significantly lower in the ASD group compared to the HC group in the density range 5% - 31% (Figure 3f).

Furthermore, we have computed two global measures that characterize how efficiently information is exchanged within a network, namely global efficiency and average local efficiency. We find that global efficiency is significantly higher ($p < 0.05$, FDR-corrected) in the ASD group compared to the HC group in the graph density range 4% - 31% (Supplementary Figure S1a). Note that the direction of the effects observed for global efficiency is opposite to the direction of effects observed for average shortest path length (Figure 3e), as global efficiency is defined as the average of reciprocal shortest path lengths between all pairs of nodes in a network. Moreover, our results for global efficiency are consistent with the results from previous studies [23, 26, 28]. We find that average local efficiency is significantly lower in the ASD group compared to the HC group in the graph density range 2%-50% (Supplementary Figure S1b). Note that the results for average local efficiency are similar to the results of average clustering coefficient (Figure 3c), since the two network measures are closely related to each other. Moreover, our results for average local efficiency are consistent with results from previous studies [23, 26, 28].

Region-specific changes in functional connectivity networks

Given the significant differences in FRC and ORC of the entire brain between the ASD group and the HC group, we evaluated node-level curvature differences in the FCNs, and determined how these differences are distributed across the 7 resting state networks (RSNs) in the brain. For this purpose, we first computed node FRC and node ORC for all the 200 nodes, across the 49 FCNs with graph densities 2% - 50% for each subject. Second, to identify the set of nodes that show significant differences between the ASD and HC groups, we compared the area under the curve (AUC) of the node FRC and the node ORC for each node using a two-tailed two-sample t-test followed by FDR correction (see Methods).

In Figure 4 and Supplementary Figure S2, we show the nodes or regions that exhibit significant differences ($p < 0.05$, FDR-corrected) in FRC and ORC, respectively, between the ASD and HC groups. We identify 83 re-

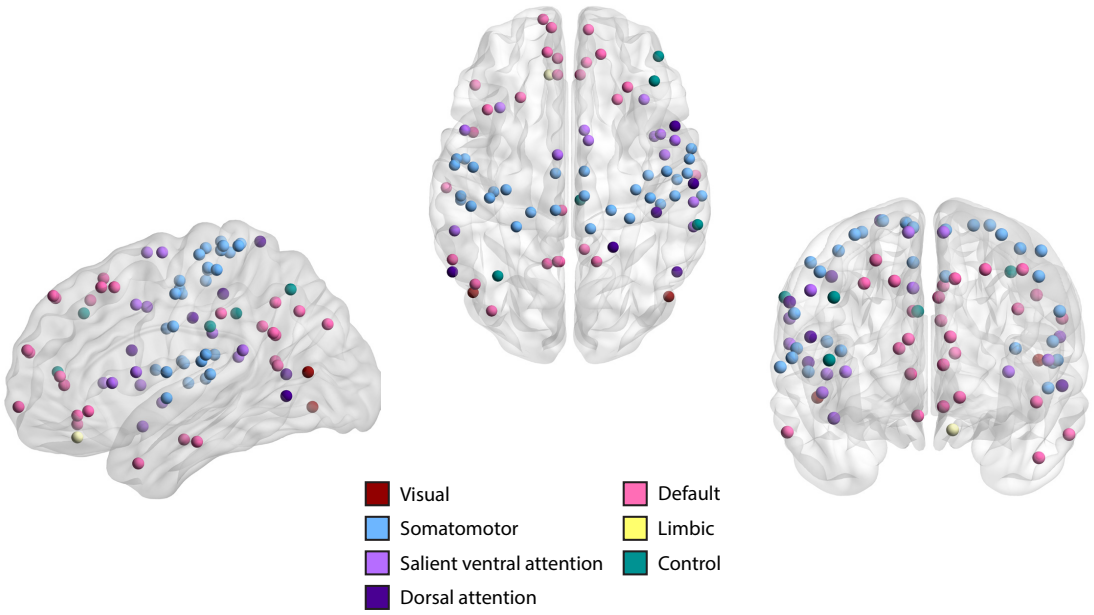

FIG. 4. Visual representation of 83 nodes or regions in the brain that are significantly different ($p < 0.05$, FDR-corrected) between individuals with autism spectrum disorder (ASD) and healthy controls (HC), as captured by Forman-Ricci curvature (FRC) of the nodes in the functional connectivity networks (FCNs) of the subjects. The nodes are defined using the Schaefer atlas and each node belongs to one of 7 resting state networks (RSNs) as listed in the figure legend. We find that identified nodes are mainly concentrated within the default network, somatomotor network, and salient ventral attention network. This figure was created using BrainNet Viewer [86].

gions that show significant between-group differences in FRC and 14 regions that show significant between-group differences in ORC. For FRC, the significant regions are spread across the 7 RSNs. However, they are mainly concentrated within 3 RSNs namely, default network (26 significant regions), somatomotor network (30 significant regions) and salient ventral attention network (13 significant regions). In the default network, RH_Default_pCunPCC_2 $(7, -49, 31)$, RH_Default_PFCdPFCm_6 $(28, 30, 43)$ and LH_Default_pCunPCC_2 $(-5, -55, 27)$ showed the lowest FDR corrected p-values. In the somatomotor network, LH_SomMot_7 $(-47, -9, 46)$, RH_SomMot_7 $(58, -5, 30)$ and LH_SomMot_10 $(-39, -24, 58)$ showed the lowest FDR corrected p-values. In the salient ventral attention network, RH_SalVentAttn_TempOccPar_2 $(60, -38, 17)$, RH_SalVentAttn_Med_3 $(9, 4, 65)$ and RH_SalVentAttn_PrC_1 $(51, 4, 40)$ showed the lowest FDR corrected p-values. For ORC, the significant regions are concentrated within the 2 RSNs namely, default network and somatomotor network. In the default network, regions LH_Default_Temp_3 $(-56 - 6, -12)$, LH_Default_PFC_4 $(-13, 63, -6)$, and RH_Default_Temp_5 $(52, -31, 2)$ exhibited the lowest FDR corrected p-values. In the somatomotor network, the region, LH_SomMot_3 $(-37, -21, 15)$ exhibits the lowest FDR corrected p value. Detailed information about the abbreviations of region names can be found at: `https://github.com/ThomasYeoLab/CBIG/tree/master/stable_projects/brain_parcellation/Schaefer2018_LocalGlobal` [54]. Thus, our node-level results for FRC and ORC suggest that the nodes or brain regions showing significant differences were not distributed evenly across the 7 RSNs, but were concentrated within the default network, somatomotor network and salient ventral attention network.

After applying both FRC and ORC to resting state FCNs in ASD and HC groups, we find that the between-group differences in FRC of the FCNs are more pronounced compared to ORC, both at the global level as well as at the level of nodes. Therefore, we mainly focus on the nodes identified using FRC in further analyses. We reiterate that the two discrete Ricci curvatures capture different aspects of the classical Ricci curvature, and thus, neither of the two measures can be treated as an alternative to the other.

a. Default

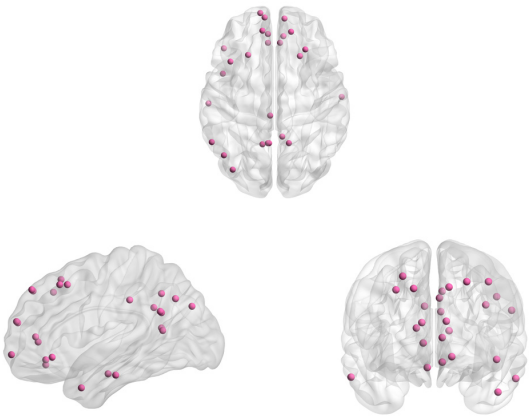

b. Somatomotor

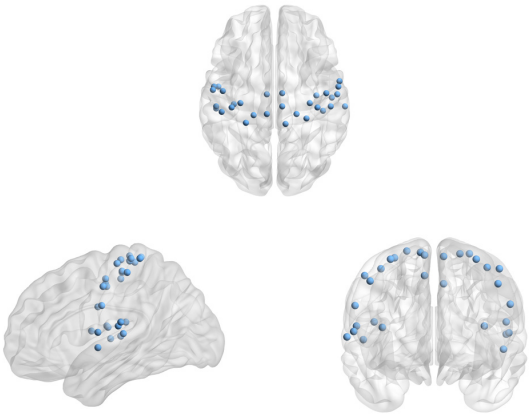

c. Salient ventral attention

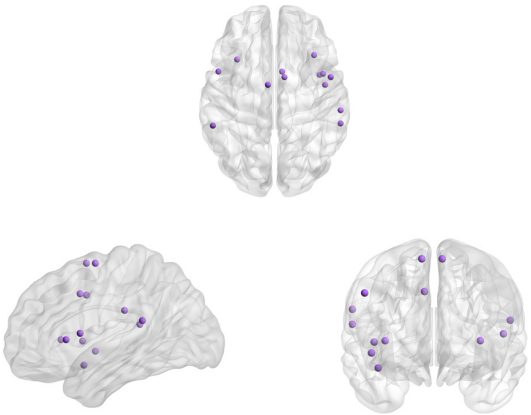

FIG. 5. Visual representations of nodes or regions in different resting state networks (RSNs) that are significantly different ($p < 0.05$, FDR-corrected) between individuals with autism spectrum disorder (ASD) and healthy controls (HC) as captured by Forman-Ricci curvature (FRC) of the nodes, and the corresponding word clouds depicting the behavioral relevance of the nodes identified in each RSN. The size of the terms in each word cloud indicates their frequency count. Note that size of the terms in each word cloud are scaled separately and thus the frequency counts cannot be compared across word clouds. (a) Nodes in the default network that show significant differences in FRC, and the corresponding word cloud. The nodes identified in the default network are associated with tasks related to social cognition and memory. (b) Nodes in the somatomotor network that show significant differences in FRC, and the corresponding word cloud. The nodes identified in the somatomotor network are associated with tasks related to movement. (c) Nodes in the salient ventral attention network that show significant differences in FRC, and the corresponding word cloud. The nodes identified in the salient ventral attention network are associated with tasks related to movement and language. In this figure, the visualizations of brain regions are created using BrainNet Viewer [86] and the word clouds are generated using wordclouds.com [87].

Behavioral relevance of region-specific changes using meta-analysis decoding

As discussed previously, we identify 83 significant regions that show significant between-group differences in FRC. Subsequently, we partitioned the set of significant brain regions according to their respective RSNs and determined the behavioral relevance of the significant regions in each RSN using Neurosynth meta-analysis (see Methods). The Neurosynth analysis enables identifying the behavioral relevance of the significant regions in an RSN more rigorously than just assuming it as the putative functional role of that RSN. The first step in the Neurosynth analysis involves identifying terms relating to cognition, perception and behavior for each significant brain region in a given RSN. The second step involves calculating the frequency counts for all the terms in an RSN. The third step involves thresholding the frequency counts of these terms with respect to the frequency counts associated with equivalent null models (see Methods).

We limit the interpretation of results from Neurosynth analysis only to default network, somatomotor network and salient ventral attention network, since a considerable number of regions are detected in these RSNs. The high number of regions with significantly different FRC in these RSNs makes the interpretation of results from these RSNs more robust to the occurrence of false positives. Another reason for considering the above-mentioned RSNs is that the regions identified in these RSNs are nearly bilaterally symmetrical. Figure 5 shows the significant brain regions separately for each of the three RSNs and the associated word clouds highlighting the behavioral relevance of the significant regions in each RSN. Supplementary Table S3 lists the significant brain regions and the terms associated with all seven RSNs.

The word cloud for the default network shows terms associated with social cognition (Figure 5a), such as 'theory-of-mind', 'social', 'social recognition', 'social cognition', 'person', 'personal' and 'personality traits'. In the default network, we can also find terms associated with memory (Figure 5a) such as 'memory', 'memories', 'memory retrieval', 'retrieval' 'recollection', 'remember', 'autobiographical memory', 'episodic memory' and 'subsequent memory'. For the somatomotor network, we find terms associated with movement (Figure 5b), such as 'motor', 'motor tasks', 'motor performance', 'movements' ,'coordination', 'limb', 'arm', 'hand movements', 'handed', 'finger', 'finger movements', 'finger tapping', 'tapping' , 'index finger', and 'force'. Finally for the salient ventral attention network, we find terms associated with movement (Figure 5c), such as 'motor', 'motor function', 'motor control', 'eye movement', 'tapping', 'mental imagery', 'imagery' and 'mirror'. For the salient ventral attention network, we also find terms associated with language (Figure 5c), such as 'phonological', 'speech', 'production', 'speech production', 'orthographic', 'articulatory', 'pseudo-words' and 'listened'.

To summarize, the regions with significantly different curvature values in each of the studied RSNs show clear behavioral relevance and are associated with social cognition (in default network), memory (in default network), movement (in somatomotor network and salient ventral attention network) and language (in salient ventral attention network).

We have also evaluated the node-level differences in two standard network measures namely, clustering coefficient and node betweenness centrality. Notably, ORC is related to clustering in networks [39]. We identify 78 brain regions that show significant differences ($p < 0.05$, FDR-corrected) in clustering coefficient, and 4 brain regions that show significant differences ($p < 0.05$, FDR-corrected) in node betweenness centrality (Supplementary Table S4). The brain regions identified by clustering coefficient are concentrated in three RSNs namely, default network, somatomotor network and salient ventral attention network (Supplementary Figure S3). Further, we computed the overlap between sets of significant brain regions identified by each of the four node-level network measures used in our study. First, we found 8 brain regions that are commonly identified by both FRC and ORC, namely, LH_SomMot_1 $(-51, -5, -2)$, LH_SomMot_3 $(-37, -21, 15)$, LH_Default_PFC_4 $(-13, 63, -6)$, RH_SomMot_3 $(38, -13, 14)$, RH_DorsAttn_Post_2 $(52, -60, 9)$, RH_SalVentAttn_FrOperIns_2 $(46, -3, -4)$, RH_SalVentAttn_TempOccPar_2 $(60, -38, 17)$ and RH_Default_Temp_2 $(61, -13, -21)$. Second, we found 71 brain regions that are commonly identified by FRC and clustering coefficient. Third, we found 5 brain regions that are commonly identified by ORC and clustering coefficient. Fourth, we found that 1 brain region is commonly identified by FRC and node betweenness centrality. Fifth, we found 2 brain regions that are commonly identified by ORC and node betweenness centrality. We do not find any brain regions that are commonly identified by clustering coefficient and node betweenness centrality.

Subsequently, we determined if there is a relationship between the curvature of brain regions that showed significant differences and clinical scores for symptom severity in ASD patients. To do this, we related the curvature of just the brain regions which showed significant differences in each RSN with the behavioral function associated with that RSN, as determined by the Neurosynth meta-analysis decoding. We performed this analysis with the curvature values and symptom severity of only the ASD patients, not the healthy controls. First, we used ADI-R social score as a measure of social cognition and related this score with the curvature of regions in the default network. Second, we used ADI-R verbal score as a measure of language and related this score with the curvature of regions in the salient ventral attention network. To test the relationship between curvature values and clinical scores, we computed partial correlations with age and gender as covariates, followed by FDR correction to control the occurrence of false

positives (see Methods). We chose the ADI-R scores among all the possible clinical scores because they are available for the most number of participants ($n = 275$) in the ASD group and the ADI-R social and ADI-R verbal scores are appropriate means to capture symptom severity in autism compared to other clinical scores [88]. Note that we also found movement-related terms in somatomotor network (Figure 5b) and salient ventral attention network (Figure 5c). However, we did not include any movement-related scores in our analysis since such scores were only available for a few participants in the ASD group.

We did not find any nodes that showed significant correlations between the curvatures (FRC and ORC) and clinical scores after FDR correction. Prior to FDR correction, FRC for the node LH_Default_Temp_1 $(-47, 8, -32)$ in the default network was positively correlated with ADI-R social score ($r = 0.122$, $p = 0.044$), FRC for the node LH_SalVentAttn_ParOper_1 $(-56, -40, 20)$ in the salient ventral attention network was positively correlated with ADI-R verbal score ($r = 0.136$, $p = 0.025$), and ORC for the node RH_Default_Temp_2 $(61, -13, -21)$ in the default network was positively correlated with ADI-R social score ($r = 0.138$, $p = 0.022$).

We also repeated the analysis for the brain regions with significantly different clustering coefficient values in the 2 RSNs namely, default network and salient ventral attention network. These brain regions show behavioral relevance and are associated with social cognition and memory in default network, and movement and language in salient ventral attention network (Supplementary Figure S4). Thus, we correlated the clustering coefficient values of significant brain regions in default network with the ADI-R social score and the clustering coefficient values of significant brain regions in salient ventral attention network with the ADI-R verbal score. In this analysis for clustering coefficient, we did not find any significant correlations with both ADI-R social scores and ADI-R verbal scores after FDR correction. To sum up, the discrete Ricci curvatures and standard network measures show no evidence for a relationship with symptom severity in ASD patients.

Validation of region-specific changes in graph Ricci curvatures using experimental evidence from non-invasive brain stimulation studies

We identified 83 brain regions that show between group differences in FRC and 14 brain regions that show between group differences in ORC. We assessed the ability of curvature measures to identify brain regions that are clinically relevant in ASD, by comparing to results from NIBS studies on ASD patients. Specifically, we performed a literature survey to identify the set of brain regions whose non-invasive stimulation using TMS or tDCS yielded positive effects on ASD symptoms. Then, we compared this set of brain regions to those with altered local graph Ricci curvature values in resting-state fMRI FCNs of ASD patients.

The studies employing TMS have reported positive effects in ASD symptoms after stimulating 4 target regions, namely, premotor cortex, dorsolateral prefrontal cortex (DLPFC), pars triangularis, and pars opercularis. The studies employing tDCS have reported positive effects in ASD symptoms after stimulating 2 target regions, namely, DLPFC and left primary motor cortex. Note that the target regions in these experiments are cortical regions that are defined differently from the ROIs (or nodes) defined in our study that are a part of the Schaefer 200 parcels atlas [54]. Therefore, in order to compare the results of our node-level analysis with the effects of stimulating the target regions, we mapped the Brodmann areas that correspond to target regions [83, 89] to the 200 Schaefer ROIs (see Methods and Supplementary Table S7).

Based on the data collected from previous NIBS experiments (Supplementary Tables S5 and S6), we identified five target regions that show evidence for improvement in behavioral or cognitive symptoms associated with ASD following TMS or tDCS, namely, premotor cortex, pars triangularis, pars opercularis, DLPFC and left primary motor cortex. These five target regions correspond to Brodmann areas 6, 45, 44, 9, 46 and 4, respectively. Note that DLPFC comprises two Broadman areas, 9 and 46 [89]. We found these Brodmann areas to encompass 31 ROIs (or nodes) in the Schaefer 200 parcels atlas. Out of these 31 ROIs, 18 ROIs also show significant ASD-related differences in FRC and 13 ROIs show significant ASD-related differences in clustering coefficient. None of these 31 ROIs show significant ASD-related differences in ORC or node betweenness centrality. A visual representation of these ROIs is provided in Figure 6. Notably, the 18 ROIs with significant ASD-related differences in FRC are a superset of the 13 ROIs with significant between-group differences in clustering coefficient. In other words, using evidence from NIBS experiments, we found that FRC is able to identify regions that are clinically relevant in ASD, that are not identified by standard network measures. Table III lists the target regions that show improvement in clinical symptoms associated with ASD following TMS or tDCS, the corresponding ROIs in the Schaefer atlas that show significant between-group differences in nodal network measures, the network measure that captured the differences, and the experimental studies that report the effects.

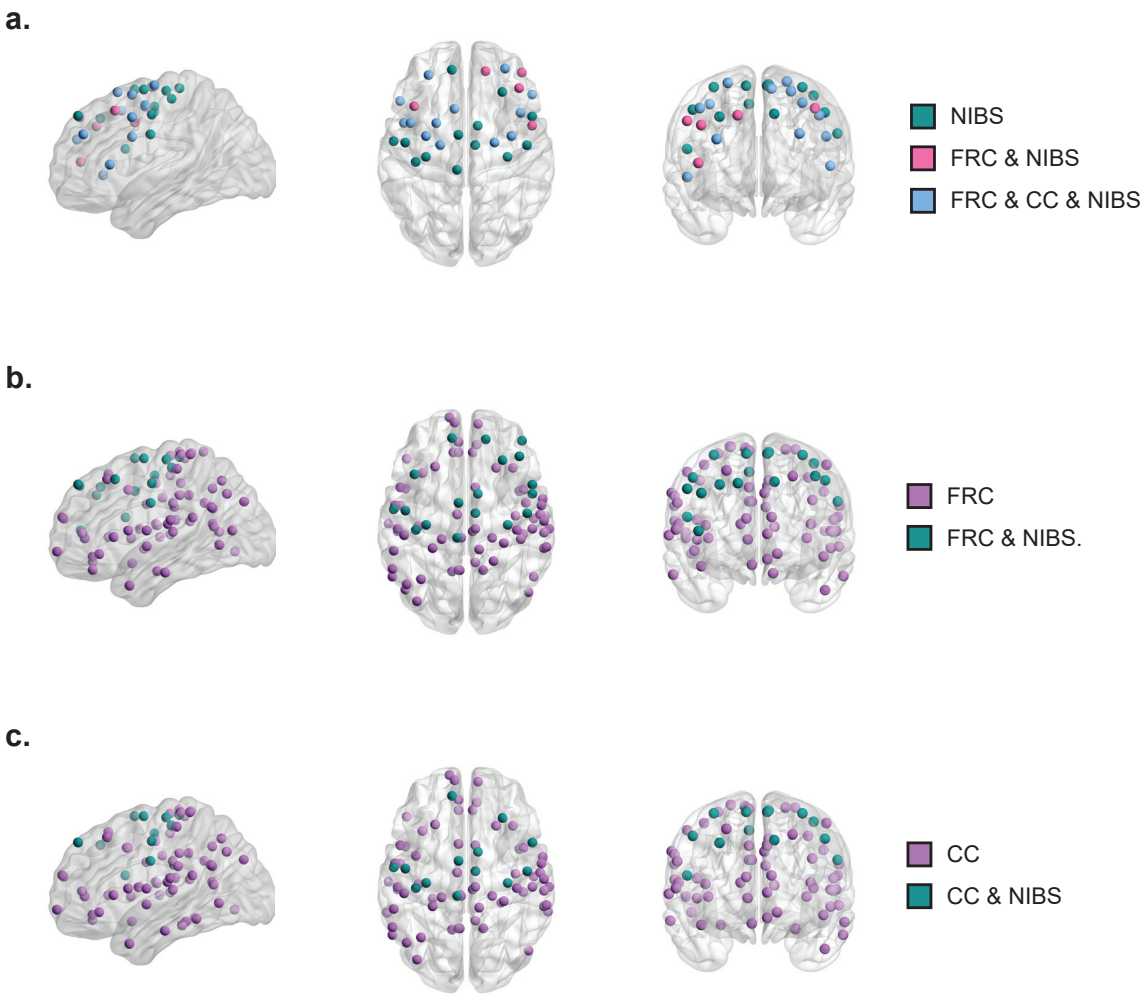

FIG. 6. Visual representation of nodes or regions with significant between-group differences in node-level network measures that exhibit improvements in clinical symptoms of ASD when stimulated, based on evidence from published NIBS experiments on subjects with ASD. (a) We found 31 nodes with experimental evidence out of which 13 nodes are identified by both FRC and clustering coefficient and 5 nodes are identified only by FRC. (b) 83 nodes identified by FRC out of which 18 nodes have experimental evidence. (c) 78 nodes identified by clustering coefficient out of which 13 nodes have experimental evidence.

Target region	Schaefer ROI	Network measure
Premotor cortex (BA 6)	RH_SalVentAttn_PrC_1	FRC
	LH_SomMot_7	FRC, CC
	LH_SomMot_12	
	LH_SalVentAttn_Med_3	
	RH_SomMot_10	
	RH_SomMot_11	
	RH_SalVentAttn_Med_3	
	RH_SomMot_14	
Pars Triangularis (Part of Broca's area) (BA 45)	RH_Cont_PFCl_3	FRC
	RH_Cont_PFCl_6	
Pars Opercularis (Part of Broca's area) (BA 44)	RH_DorsAttn_PrCv_1	FRC, CC
Dorsolateral prefrontal cortex (BA 9 and BA 46)	LH_Default_PFC_11	FRC
	RH_Default_PFCdPFCm_5	
	LH_Default_PFC_9	FRC, CC
	RH_Default_PFCdPFCm_6	
Left primary motor cortex (left M1) (BA 4)	LH_SomMot_6	FRC, CC
	LH_SomMot_10	
	LH_SomMot_15	

TABLE III. The list of the target brain regions that show improvement in clinical symptoms associated with ASD following TMS or tDCS procedure, the corresponding ROIs in the Schaefer atlas that show significant between-group differences in node-level network measures, the network measure that captured the differences (Forman-Ricci curvature (FRC), clustering coefficient (CC)), and the experimental studies that report the effects. Detailed methodology and reported effects of the experimental studies are presented in Supplementary Tables S5 and S6.

DISCUSSION

Graph Ricci curvatures have not been previously applied to study altered resting-state functional connectivity in ASD. In the present work, we used two notions of graph Ricci curvature, namely Forman-Ricci curvature (FRC) and Ollivier-Ricci curvature (ORC) to compare the resting-state FCNs of individuals with ASD relative to healthy controls. To the best of our knowledge, this is the first work involving the application of multiple notions of graph Ricci curvature to analyse brain connectivity. We found that average edge curvature can effectively be used to compare the whole-brain functional connectivity of individuals in the ASD and HC groups. Additionally, we studied the differences in node curvature between the two groups and identified specific regions in the brain responsible for altered functional connectivity in ASD.

We acquired rs-fMRI scans of 1112 participants as provided by the ABIDE-I project [15]. The large sample size of the ABIDE-I dataset offers substantial statistical power, thereby increasing the reliability of the reported results [2, 11, 15]. We preprocessed each scan using the CONN functional connectivity toolbox [53], implementing thorough quality assessment (QA) checks both before and after preprocessing. For each participant, we generated a 200×200 functional connectivity (FC) matrix using Schaefer atlas [54] and constructed FCNs with a broad range of edge densities using a maximum spanning tree (MST) followed by sparsity-based thresholding. A MST is particularly useful for network-based analyses since it ensures that the resulting network is always connected. Similar network construction approaches involving spanning trees have previously been used for financial networks [41, 42] and brain FCNs [72].

After comparing the average edge curvatures of the FCNs in the ASD and HC groups, we found reduced average FRC and average ORC in individuals with ASD. Similar analysis using standard network measures revealed reduced average clustering coefficient, reduced modularity, reduced average path length, reduced average node betweenness centrality, increased global efficiency and reduced average local efficiency. All the standard network measures except node betweenness centrality have previously been used to study brain-wide changes in functional connectivity in ASD [23, 26, 28], and our results are in agreement with previous findings. However, the changes in graph Ricci curvatures have not previously been studied for FCNs in ASD. Our results illustrate the sensitivity of graph Ricci curvatures, especially FRC, in discriminating the resting state FCNs of individuals with ASD compared to HC.

After comparing the node curvatures of the FCNs in the ASD and HC groups, we identified 83 brain regions that are significantly different in FRC and 14 brain regions that are significantly different in ORC between the two groups. Both FRC and ORC commonly identify 5 regions. Moreover, we found that these regions are bilaterally symmetrical and mainly concentrated in 3 RSNs namely, default network, somatomotor network and salient ventral attention network. Previously, Farooq *et al.* [45] have used ORC to compare structural connectivity networks of individuals with ASD relative to HC, and showed that regions with significant difference in ORC are present in visual, dorsal

attention, ventral attention areas and temporal lobe. Our results from comparing ORC of resting state FCNs in ASD reveal regions in visual network, dorsal attention network, salient ventral attention network, and additional regions in default network, somatomotor network and limbic network.

As a post hoc analysis, we performed Neurosynth meta-analysis to interpret the behavioral relevance of the brain regions in each RSN with significant differences in curvature. The Neurosynth analysis reveals specific cognitive functions associated with the regions identified in a given RSN, which can then be used to test hypotheses about how node curvatures relate to behavioral scores. Among the regions with significant differences in curvature, we found that the regions in default network are related to memory and social cognition, the regions in somatomotor network are related to movement and the regions in salient ventral attention network are related to movement and language. Notably, Farooq *et. al* [45] have used ORC to compare structural connectivity networks of individuals with ASD relative to HC, and showed that regions with significant difference in ORC are related to semantic memory, socially relevant memories, emotions and visual perception.

Thereafter, we determined if there is a relationship between the curvature of brain regions that showed significant differences and ADI-R scores for symptom severity in ASD patients. We found that discrete Ricci curvatures and standard network measures show no evidence for a relationship with symptom severity in ASD patients. Our results are in agreement with previous graph-theoretic studies on FCNs in the ABIDE dataset, which also report moderate or no correlation between node-level network measures and symptom severity scores for the ASD group [26, 27, 29, 90]. Notably, Keown *et al.* [27] have carefully chosen high quality fMRI images from ABIDE-I dataset and computed global and node-level measures on the resulting FCNs. They reported no significant correlations between the network measures and symptom severity scores for the ASD group, and further cautioned about the interpretation of their results, as the correlation analysis could be confounded by site differences in age ranges. We would also like to emphasize that the ADI-R scores used in our study were unavailable for 120 out of 395 participants in the ASD group.

We demonstrate that graph Ricci curvatures identify regions whose stimulation using non-invasive technologies, e.g. TMS, have been shown to result in a positive effect on ASD symptoms of patients. To our knowledge, this is the first instance of external validation of the clinical significance of regions identified by local graph-theoretic measures with respect to the literature on experiments with non-invasive stimulation technologies. We further note that the set of regions identified by other local graph-theoretic measures, e.g. clustering coefficient, which overlap with those regions identified by non-invasive stimulation, are a subset of the set of regions identified by FRC which overlap with regions identified by non-invasive stimulation. These results commend the use of graph Ricci curvatures to generate hypotheses about the clinical significance of brain regions in conditions such as ASD, which can then be tested by stimulating these regions with non-invasive technologies, e.g. TMS [85, 91, 92].

There was a significant difference in the IQ scores between the ASD and HC groups, which introduces a potential confound to our analysis. Previous studies involving graph-theoretic analysis of rs-fMRI scans in the ABIDE dataset have matched the groups on IQ scores [27, 28, 90]. However, we choose to include all subjects in our analysis rather than sub-selecting ASD subjects according to IQ, since sub-selecting would make ASD cohort less representative and the results of our analyses would be less generalizable to the typical ASD population [59]. Confining the analysis to IQ-matched ASD patients would include only high-functioning ASD patients in the analyses, hence, our results would not be generalizable to ASD subjects whose cognitive functioning is more severely affected. In addition, we have not included IQ as a covariate while comparing the global and local network measures across groups. However, Dennis *et al.* [59] have shown that using IQ as a matching variable or covariate during studies of neurodevelopmental disorders could lead to anomalous findings about neurocognitive function.

To sum up, we find that geometric notions of graph Ricci curvature can be effectively used to determine global and node-level changes in functional connectivity networks of individuals with ASD. We have also shown that the node-level changes captured by FRC could be clinically significant. The methods used in the present work could further be explored to study functional connectivity networks in other atypical populations. Additionally, since graph Ricci curvatures are fundamentally defined on edges, future studies could be aimed at devising edge-based methods to analyze brain functional or structural connectivity.

ACKNOWLEDGEMENTS

We would like to thank Linda Geerligs for discussions. A.S. would like to thank Max Planck Society, Germany for research support via a Max Planck Partner Group in Mathematical Biology. E.S. and J.J. acknowledge support from the German-Israeli Foundation (GIF) grant no. I-1514-304.6/2019.

ADDITIONAL INFORMATION

Competing interests The authors declare no competing interests.

Supplementary Information accompanies the paper.

Data Availability All data generated or analyzed during this study and the associated programs are included in the article or are publicly available from the dedicated GitHub repository: `https://github.com/asamallab/Curvature-FCN-ASD`.

[1] National Institute of Neurological Disorders and Stroke. Autism Spectrum Disorder Fact Sheet (2020).
[2] C. Lord, T. S. Brugha, T. Charman, J. Cusack, G. Dumas, *et al.*, Nature Reviews Disease Primers **6**, 5 (2020).
[3] K. Wang, H. Gaitsch, H. Poon, N. J. Cox, and A. Rzhetsky, Nature Genetics **49**, 1319 (2017).
[4] M. J. Maenner, K. A. Shaw, J. Baio, EdS1, A. Washington, *et al.*, MMWR. Surveillance Summaries **69**, 1 (2020).
[5] N. K. Arora, M. K. C. Nair, S. Gulati, V. Deshmukh, A. Mohapatra, *et al.*, PLOS Medicine **15**, e1002615 (2018).
[6] D. Fein, M. Barton, I.-M. Eigsti, E. Kelley, L. Naigles, *et al.*, Journal of Child Psychology and Psychiatry **54**, 195 (2013).
[7] M. Langen, D. Bos, S. D. Noordermeer, H. Nederveen, H. van Engeland, *et al.*, Biological Psychiatry **76**, 405 (2014).
[8] N. D. Woodward and C. J. Cascio, JAMA Psychiatry **72**, 743 (2015).
[9] S. Solso, R. Xu, J. Proudfoot, D. J. Hagler, K. Campbell, *et al.*, Biological Psychiatry **79**, 676 (2016).
[10] C. C. Clements, A. R. Zoltowski, L. D. Yankowitz, B. E. Yerys, R. T. Schultz, *et al.*, JAMA Psychiatry **75**, 797 (2018).
[11] J. V. Hull, L. B. Dokovna, Z. J. Jacokes, C. M. Torgerson, A. Irimia, *et al.*, Frontiers in Psychiatry **7**, 205 (2017).
[12] N. K. Logothetis, Nature **453**, 869 (2008).
[13] B. Biswal, F. Zerrin Yetkin, V. M. Haughton, and J. S. Hyde, Magnetic resonance in medicine **34**, 537 (1995).
[14] M. E. Raichle, A. M. MacLeod, A. Z. Snyder, W. J. Powers, D. A. Gusnard, *et al.*, Proceedings of the National Academy of Sciences **98**, 676 (2001).
[15] A. Di Martino, C.-G. Yan, Q. Li, E. Denio, F. X. Castellanos, *et al.*, Molecular Psychiatry **19**, 659 (2014).
[16] E. Bullmore and O. Sporns, Nature Reviews Neuroscience **10**, 186 (2009).
[17] M. Rubinov and O. Sporns, Neuroimage **52**, 1059 (2010).
[18] D. Van Essen, K. Ugurbil, E. Auerbach, D. Barch, T. Behrens, *et al.*, NeuroImage **62**, 2222 (2012).
[19] O. Sporns, NeuroImage **80**, 53 (2013).
[20] F. V. Farahani, W. Karwowski, and N. R. Lighthall, Frontiers in Neuroscience **13**, 585 (2019).
[21] J. S. Anderson, J. A. Nielsen, M. A. Ferguson, M. C. Burback, E. T. Cox, *et al.*, NeuroImage: Clinical **2**, 703 (2013).
[22] E. Redcay, J. M. Moran, P. L. Mavros, H. Tager-Flusberg, J. D. E. Gabrieli, *et al.*, Frontiers in Human Neuroscience **7**, 10.3389/fnhum.2013.00573 (2013).
[23] J. Rudie, J. Brown, D. Beck-Pancer, L. Hernandez, E. Dennis, *et al.*, NeuroImage: Clinical **2**, 79 (2013).
[24] X. You, M. Norr, E. Murphy, E. S. Kuschner, E. Bal, *et al.*, Frontiers in Human Neuroscience **7**, 10.3389/fnhum.2013.00482 (2013).
[25] S. Ray, M. Miller, S. Karalunas, C. Robertson, D. S. Grayson, *et al.*, Human Brain Mapping **35**, 6032 (2014).
[26] T. Itahashi, T. Yamada, H. Watanabe, M. Nakamura, D. Jimbo, *et al.*, PLoS ONE **9**, e94115 (2014).
[27] C. L. Keown, M. C. Datko, C. P. Chen, J. O. Maximo, A. Jahedi, *et al.*, Biological Psychiatry: Cognitive Neuroscience and Neuroimaging **2**, 66 (2017).
[28] V. Harlalka, R. S. Bapi, P. K. Vinod, and D. Roy, Brain Connectivity **8**, 407 (2018).
[29] L. Chen, Y. Chen, H. Zheng, B. Zhang, F. Wang, *et al.*, Brain Imaging and Behavior **15**, 1058 (2021).
[30] M. Boguñá, I. Bonamassa, M. De Domenico, S. Havlin, D. Krioukov, *et al.*, Nature Reviews Physics **3**, 114 (2021).
[31] A. P. Kartun-Giles and G. Bianconi, Chaos, Solitons & Fractals: X **1**, 100004 (2019).
[32] I. Iacopini, G. Petri, A. Barrat, and V. Latora, Nature communications **10**, 1 (2019).
[33] G. Bianconi, *Higher-Order Networks*, Elements in Structure and Dynamics of Complex Networks (Cambridge University Press, 2021).
[34] J. Jost, *Riemannian geometry and geometric analysis*, 7th ed. (Springer Berlin Heidelberg, New York, NY, 2017).
[35] B. Chow and F. Luo, Journal of Differential Geometry **63**, 10.4310/jdg/1080835659 (2003).
[36] R. Forman, Discrete and Computational Geometry **29**, 323 (2003).
[37] Y. Ollivier, Comptes Rendus Mathematique **345**, 643 (2007).
[38] R. P. Sreejith, K. Mohanraj, J. Jost, E. Saucan, and A. Samal, Journal of Statistical Mechanics: Theory and Experiment **2016**, 063206 (2016).
[39] A. Samal, R. P. Sreejith, J. Gu, S. Liu, E. Saucan, *et al.*, Scientific Reports **8**, 8650 (2018).
[40] R. Sandhu, T. Georgiou, E. Reznik, L. Zhu, I. Kolesov, *et al.*, Scientific Reports **5**, 12323 (2015).
[41] R. S. Sandhu, T. T. Georgiou, and A. R. Tannenbaum, Science Advances **2**, e1501495 (2016).
[42] A. Samal, H. K. Pharasi, S. J. Ramaia, H. Kannan, E. Saucan, *et al.*, Royal Society Open Science **8**, rsos.201734, 201734 (2021).
[43] J. Sia, E. Jonckheere, and P. Bogdan, Scientific Reports **9**, 9800 (2019).

[44] C.-C. Ni, Y.-Y. Lin, F. Luo, and J. Gao, Scientific Reports **9**, 9984 (2019).
[45] H. Farooq, Y. Chen, T. T. Georgiou, A. Tannenbaum, and C. Lenglet, Nature Communications **10**, 4937 (2019).
[46] A. K. Simhal, K. L. H. Carpenter, S. Nadeem, J. Kurtzberg, A. Song, *et al.*, Scientific Reports **10**, 10819 (2020).
[47] H. Farooq, C. Lenglet, and F. Nelson, Frontiers in Neurology **11**, 606478 (2020).
[48] T. Chatterjee, R. Albert, S. Thapliyal, N. Azarhooshang, and B. DasGupta, Scientific Reports **11**, 8121 (2021).
[49] M. Weber, J. Stelzer, E. Saucan, A. Naitsat, G. Lohmann, *et al.*, arXiv:1707.00180 [cs, q-bio] (2019), arXiv: 1707.00180.
[50] G. Lohmann, E. Lacosse, T. Ethofer, V. J. Kumar, K. Scheffler, *et al.*, *Predicting intelligence from fMRI data of the human brain in a few minutes of scan time*, preprint (Neuroscience, 2021).
[51] M. Hallett, Neuron **55**, 187 (2007).
[52] M. A. Nitsche, L. G. Cohen, E. M. Wassermann, A. Priori, N. Lang, *et al.*, Brain stimulation **1**, 206 (2008).
[53] S. Whitfield-Gabrieli and A. Nieto-Castanon, Brain Connectivity **2**, 125 (2012).
[54] A. Schaefer, R. Kong, E. M. Gordon, T. O. Laumann, X.-N. Zuo, *et al.*, Cerebral Cortex **28**, 3095 (2018).
[55] T. Yarkoni, R. A. Poldrack, T. E. Nichols, D. C. Van Essen, and T. D. Wager, Nature Methods **8**, 665 (2011).
[56] N. Williams, S. Wang, G. Arnulfo, L. Nobili, S. Palva, *et al.*, *Modules in connectomes of phase-synchronization comprise anatomically contiguous, functionally related regions*, preprint (Neuroscience, 2021).
[57] Freepik from www.flaticon.com (2021).
[58] C. Cameron, B. Yassine, C. Carlton, C. Francois, E. Alan, *et al.*, Frontiers in Neuroinformatics **7**, 10.3389/conf.fninf.2013.09.00041 (2013).
[59] M. Dennis, D. J. Francis, P. T. Cirino, R. Schachar, M. A. Barnes, *et al.*, Journal of the International Neuropsychological Society **15**, 331 (2009).
[60] J. L. Andersson, C. Hutton, J. Ashburner, R. Turner, and K. Friston, NeuroImage **13**, 903 (2001).
[61] R. Sladky, K. J. Friston, J. Tröstl, R. Cunnington, E. Moser, *et al.*, NeuroImage **58**, 588 (2011).
[62] J. Ashburner and K. J. Friston, NeuroImage **26**, 839 (2005).
[63] X. J. Chai, A. N. Castañón, D. Öngür, and S. Whitfield-Gabrieli, NeuroImage **59**, 1420 (2012).
[64] K. J. Friston, S. Williams, R. Howard, R. S. J. Frackowiak, and R. Turner, Magnetic Resonance in Medicine **35**, 346 (1996).
[65] J. D. Power, A. Mitra, T. O. Laumann, A. Z. Snyder, B. L. Schlaggar, *et al.*, NeuroImage **84**, 320 (2014).
[66] R. Ciric, D. H. Wolf, J. D. Power, D. R. Roalf, G. L. Baum, *et al.*, NeuroImage **154**, 174 (2017).
[67] A. I. Luppi and E. A. Stamatakis, Network Neuroscience **5**, 96 (2021).
[68] J. B. Kruskal, Proceedings of the American Mathematical Society **7**, 48 (1956).
[69] S. Achard and E. Bullmore, PLoS Computational Biology **3**, e17 (2007).
[70] D. S. Bassett, B. G. Nelson, B. A. Mueller, J. Camchong, and K. O. Lim, NeuroImage **59**, 2196 (2012).
[71] T. Xu, K. R. Cullen, B. Mueller, M. W. Schreiner, K. O. Lim, *et al.*, NeuroImage: Clinical **11**, 302 (2016).
[72] S. Achard, C. Delon-Martin, P. E. Vertes, F. Renard, M. Schenck, *et al.*, Proceedings of the National Academy of Sciences **109**, 20608 (2012).
[73] V. D. Blondel, J.-L. Guillaume, R. Lambiotte, and E. Lefebvre, Journal of Statistical Mechanics: Theory and Experiment **2008**, P10008 (2008).
[74] V. Latora and M. Marchiori, Physical Review Letters **87**, 198701 (2001).
[75] Y. Benjamini and Y. Hochberg, Journal of the Royal Statistical Society: Series B (Methodological) **57**, 289 (1995).
[76] A. A. Hagberg, D. A. Schult, and P. J. Swart, in *Proceedings of the 7th Python in Science Conference*, edited by G. Varoquaux, T. Vaught, and J. Millman (Pasadena, CA USA, 2008) pp. 11 – 15.
[77] P. Virtanen, R. Gommers, T. E. Oliphant, M. Haberland, T. Reddy, *et al.*, Nature Methods **17**, 261 (2020).
[78] S. Seabold and J. Perktold, in *9th Python in Science Conference* (2010).
[79] C. Lord, M. Rutter, and A. Le Couteur, Journal of Autism and Developmental Disorders **24**, 659 (1994).
[80] D. Moher, A. Liberati, J. Tetzlaff, D. G. Altman, and P. Group, PLoS medicine **6**, e1000097 (2009).
[81] J. B. Barahona-Corrêa, A. Velosa, A. Chainho, R. Lopes, and A. J. Oliveira-Maia, Frontiers in integrative neuroscience **12**, 27 (2018).
[82] S. García-González, J. Lugo-Marín, I. Setien-Ramos, L. Gisbert-Gustemps, G. Arteaga-Henríquez, *et al.*, European Neuropsychopharmacology (2021).
[83] M. Strotzer, Clinical Neuroradiology **19**, 179 (2009).
[84] C. Rorden, H.-O. Karnath, and L. Bonilha, Journal of cognitive neuroscience **19**, 1081 (2007).
[85] C. J. Lynch, A. L. Breeden, E. M. Gordon, J. B. C. Cherry, P. E. Turkeltaub, *et al.*, Cerebral Cortex **29**, 3912 (2018), https://academic.oup.com/cercor/article-pdf/29/9/3912/29104735/bhy270.pdf.
[86] M. Xia, J. Wang, and Y. He, PloS one **8**, e68910 (2013).
[87] wordclouds.com : Free online word cloud generator and tag cloud creator (2021).
[88] J. Lefort-Besnard, K. Vogeley, L. Schilbach, G. Varoquaux, B. Thirion, *et al.*, Translational Psychiatry **10**, 257 (2020).
[89] E. C. Cieslik, K. Zilles, S. Caspers, C. Roski, T. S. Kellermann, *et al.*, Cerebral cortex **23**, 2677 (2013).
[90] Y. Lee, B.-y. Park, O. James, S.-G. Kim, and H. Park, Frontiers in Human Neuroscience **11**, 418 (2017).
[91] M. V. Sale, J. B. Mattingley, A. Zalesky, and L. Cocchi, Neuroscience & Biobehavioral Reviews **57**, 187 (2015).
[92] J. Downar, D. M. Blumberger, and Z. J. Daskalakis, Trends in cognitive sciences **20**, 107 (2016).